J Biomol NMR (2010) 47:183–194
DOI 10.1007/s10858-010-9422-z

ARTICLE

MQ-HNCO-TROSY for the measurement of scalar and residual dipolar couplings in larger proteins: application to a 557-residue IgFLNa16-21

Sampo Mäntylahti · Outi Koskela · Pengju Jiang · Perttu Permi

Received: 22 December 2009 / Accepted: 14 April 2010 / Published online: 8 May 2010

Abstract We describe a novel pulse sequence, MQ-HNCO-TROSY, for the measurement of scalar and residual dipolar couplings between amide proton and nitrogen in larger proteins. The experiment utilizes the whole $2T_N$ polarization transfer delay for labeling of ^{15}N chemical shift in a constant time manner, which efficiently doubles the attainable resolution in ^{15}N dimension with respect to the conventional HNCO-TROSY experiment. In addition, the accordion principle is employed for measuring $(J + D)_{NH}$s, and the multiplet components are selected with the generalized version of the TROSY scheme introduced by Nietlispach (J Biomol NMR 31:161–166, 2005). Therefore, cross peak overlap is diminished while the time period during which the ^{15}N spin is susceptible to fast transverse relaxation associated with the anti-TROSY transition is minimized per attainable resolution unit. The proposed MQ-HNCO-TROSY scheme was employed for measuring RDCs in high molecular weight protein IgFLNa16-21 of 557 residues, resulting in 431 experimental RDCs. Correlations between experimental and back-calculated RDCs in individual domains gave relatively low Q-factors (0.19–0.39), indicative of sufficient accuracy that can be obtained with the proposed MQ-HNCO-TROSY experiment in high molecular weight proteins.

Keywords Dipolar couplings · HNCO · NMR · Proteins · Scalar couplings · TROSY

S. Mäntylahti · P. Permi (✉)
NMR Laboratory, Program in Structural Biology and Biophysics, Institute of Biotechnology/NMR Laboratory, University of Helsinki, P.O. Box 65, 00014 Helsinki, Finland
e-mail: Perttu.Permi@helsinki.fi

O. Koskela
Laboratory of Organic Chemistry, Department of Chemistry, University of Helsinki, P.O. Box 55, 00014 Helsinki, Finland

P. Jiang
Biochemistry Department, University of Oxford, Oxford OX1 3QU, UK

Introduction

Introduction of tunable alignment of proteins in a dilute liquid crystal medium gives rise to residual dipolar couplings (RDCs), which have revolutionized structural characterization of biological macromolecules (Blackledge 2005; Tjandra and Bax 1997; Bouvignies et al. 2007; Prestegard et al. 2000). RDCs are direct product between gyromagnetic ratios of two nuclei, and the magnitude of the coupling is depended on both the bond vector orientation and the internuclear distance (Annila and Permi 2004). RDCs enable not only determination of macromolecular structures with higher precision but also studies of conformational changes (Pääkkönen et al. 2000), domain orientation (Fischer et al. 1999; Tugarinov and Kay 2003), dynamics and folding (Fredriksson et al. 2004; Lakomek et al. 2006; Tolman and Ruan 2006). Effective application of these orientational restraints necessitates accurately determined residual dipolar contribution (D), which can be derived from measurements of scalar (J) splittings in water and ($J + D$) splittings in the presence of orienting medium. The accuracy is often compromised due to additional line broadening of NMR signals induced not only by dipole–dipole (DD) relaxation, but also by non-averaged dipolar contribution (RDCs) in aligned medium, from proximate protons. For this reason, higher accuracy is typically obtained when ($J + D$) splitting is measured from heteronuclear dimension instead of directly detected proton dimension. One-bond RDC between the amide proton and nitrogen ($^1D_{NH}$) can be measured with modest effort and high accuracy in case of small to medium sized proteins. To that end, several two-dimensional experiments have been developed, which utilize the well-dispersed ^{15}N, ^{1}H correlation map together with the spin-state separation of up- or downfield ^{15}N–^{1}H multiplet components into the subspectra, which eliminates additional spectral crowding due to increased number of cross peaks in J coupled experiments (Meissner et al. 1997; Ottiger et al. 1998; Andersson et al. 1998; Weigelt 1998; Lerche et al. 1999; Permi 2002; Würtz and Permi, 2007). However, in case of larger proteins (>30–40 kDa), the accurate measurement of J_{NH} and $(J + D)_{NH}$ coupling becomes much more difficult due to increasing number of cross peaks and the drastic difference in decay rates between the so-called TROSY and anti-TROSY components of the ^{15}N–^{1}H multiplet (Pervushin et al. 1997; Yang and Kay 1999; Kontaxis et al. 2000). Although position of the TROSY component of the ^{15}N–^{1}H multiplet can be measured with high accuracy, a relative position of the ^{15}N shift associated with ^{1}H$^{\beta}$ spin state is vaguer due to broader line and lower sensitivity of the anti-TROSY component. Increased spectral overlap, together with decreased sensitivity and line broadening in high molecular weight systems, makes measurement of RDCs in these proteins very challenging. To this end Kay and coworkers have proposed HNCO-TROSY based experiment for measuring $(J + D)_{NH}$s, which provides enhanced cross peak dispersion when compared to two-dimensional ^{15}N-HSQC or ^{15}N-TROSY based experiments (Yang et al. 1999).

In this work, we introduce a modified HNCO-based pulse sequence, which offers superior resolution in ^{15}N dimension in comparison to traditional HNCO-TROSY experiment and is especially useful for measuring RDCs between amide proton and nitrogen in high molecular weight proteins. The proposed pulse sequence was evaluated with three proteins, 56-residue GB1, 76-residue human ubiquitin, and a 557-residue (60 kDa) filamin A, composed of six consecutive (16–21) filamin-type immunoglobulin-like (IgFLN) domains.

Results and discussion

Proposed pulse sequence for the measurement of $(J + D)_{HN}$ couplings in ^{15}N, ^{13}C (^{2}H) labeled proteins is depicted in Fig. 1. The experiment mostly resembles well-described HNCO-TROSY experiments i.e. it establishes correlations between ^{1}H^N, ^{15}N spins, and ^{13}C′ nucleus of the preceding residue (Salzmann et al. 1998; Yang and Kay 1999). However, some of the common features of the original scheme have been modified for the purpose of measuring RDCs in larger proteins. These changes will be briefly described in the following:

The experiment starts with the ^{1}H–^{15}N INEPT, which transfers magnetization from ^{1}H to ^{15}N (time point a). This is followed by the delay 2T$_N$ during which the antiphase coherence between ^{15}N(i) and ^{13}C′(i – 1) is established. At time point b, 90°(^{13}C′) pulse converts magnetization into the ^{15}N–^{13}C′ multiple-quantum (MQ) coherence. During the ensuing t$_1$ period, the ^{13}C′ chemical shift is allowed to evolve, whereas 180°(^{15}N) pulse at the midpoint of t$_1$ period refocuses ^{15}N chemical shift evolution. At time point c, 90°(^{13}C′) pulse transforms magnetization back to the ^{15}N single-quantum (SQ) coherence, which evolves under the ^{15}N chemical shift Hamiltonian during the t$_2$ period. After chemical shift labeling of ^{15}N, the desired ^{15}N SQ coherence is transferred to amide proton for detection, using the gradient selected and sensitivity enhanced TROSY block recently introduced by Nietlispach (2005), which suppresses the anti-TROSY pathway that plagued the original scheme proposed by Yang and Kay (1999). After Fourier transformation of time domain signal, this results in a familiar HNCO-TROSY spectrum with cross peaks emerging at $\omega_{C'}$, $\omega_N - \pi J_{NH}$, and $\omega_{HN} + \pi J_{NH}$ frequencies. Hence, we dub this experiment as MQ-HNCO-TROSY.

In comparison to the conventional HNCO-TROSY scheme, the MQ-HNCO-TROSY experiment utilizes the whole 2T$_N$ period instead of T$_N$ period for the ^{15}N chemical shift labeling, thus enabling use of two-fold higher experimental resolution in the ^{15}N dimension, which is absolutely critical in case of high molecular weight proteins with hundreds of residues. Multiple-quantum ^{15}N–^{13}C coherence transfer scheme has earlier been proposed by Wüthrich and co-workers (Salzmann et al. 1998) and by Clore and colleagues (Hu et al. 2009) but we prefer using the full sweep implementation (Madsen et al. 1993; Puttonen et al. 2006) which yields better sensitivity, resolution and precision when measuring RDCs.

In this work, we have employed a generalized version of the TROSY scheme by Nietlispach (2005) i.e. the proposed pulse sequence utilizes a spin-state selective filter that can be used to select any of the four possible ^{15}N–^{1}H multiplet components by changing the phase of the first ^{1}H(ϕ_3) and the last ^{15}N(ϕ_4) pulse in the TROSY filter (see legend to Fig. 1 for details). This was motivated by earlier studies by us and others to measure RDCs in directly detected ^{1}H dimension (Lerche et al. 1999; Permi 2002; Würtz and Permi 2007). Indeed, measuring ^{15}N–^{1}H couplings from ^{1}H dimension either between TROSY and anti-TROSY lines or between the TROSY and decoupled (HSQC) component might be an attractive possibility, especially on large proteins and highly perdeuterated samples. However, initial testing with large 60 kDa protein in a dilute liquid crystal medium at 800 MHz revealed that, as earlier reported by Bax and co-workers (Kontaxis et al. 2000), measuring the

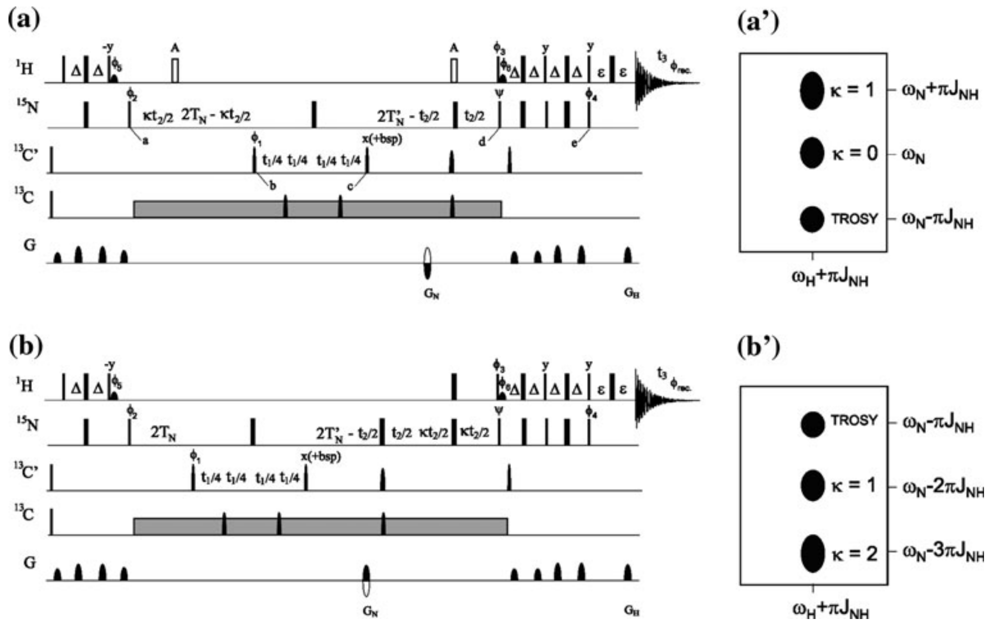

Fig. 1 **a** MQ-HNCO-TROSY and **b** modified HR-TROSY HNCO (Hu et al. 2009) pulse sequences for measuring $^1(J + D)_{NH}$. Narrow and wide bars correspond to rectangular 90° and 180° pulses, with phase x unless otherwise indicated, respectively. 90° (180°) pulses for $^{13}C'$ are applied with a strength of $\Omega/\sqrt{15}$ ($\Omega/\sqrt{3}$), where Ω is the frequency difference between the centers of the $^{13}C'$ and the aliphatic $^{13}C^{\alpha}$ regions. The ^1H, ^{15}N, and $^{13}C'$ carrier positions are 4.7 (H_2O), 120 (center of ^{15}N spectral region), and 175 ppm (center of $^{13}C'$ spectral region), respectively. The semi-selective decoupling for removal of $^{13}C'$–$^{13}C^{\alpha}$ and ^{15}N–$^{13}C^{\alpha}$ coupling interactions during t_1 and t_2, respectively, can be accomplished using either the SEDUCE-1 decoupling sequence (McCoy and Mueller 1992) or three 180° $^{13}C'$ rectangular or one-lobe sinc pulses (indicated as half ellipsoids) applied off-resonance with phase modulation by Ω. Pulsed field gradients are inserted as indicated for coherence transfer pathway selection and residual water suppression. The delays employed are: $\Delta = 1/(4J_{NH})$; $2T_N = 1/(2J_{NC'}) = 24 - 34$ ms; ε = gradient+field recovery delay. The TROSY component is recorded by omitting all 180°(^1H) pulses between time points a and d with the following phase cycling: $\phi_1 = x, -x$; $\phi_2 = x$; $\phi_3 = x$; $\phi_4 = y$; $\phi_5 = x$; $\phi_6 = x$; $\psi = x$; $\phi_{rec} = x, -x$. The pure anti-TROSY component along ^{15}N dimension can be selected by changing the phases ϕ_3 and ϕ_6 to $-x$. If desired, the anti-TROSY component instead of TROSY component in ^1H dimension can be selected by inverting the phase of ϕ_4. The downscaled anti-TROSY component is obtained by recording the experiment (**a**) with the 180°(^1H) pulses given at points A, and using the phase cycling: $\phi_1 = x, -x$; $\phi_2 = x$, $\phi_3 = x$; $\phi_4 = -y$; $\phi_5 = -x$; $\phi_6 = -x$; $\psi = -x$; $\phi_{rec} = x, -x$. If the up-scaled anti-TROSY component is measured using the modified HR-TROSY HNCO (Hu et al. 2009) scheme (**b**), the phase cycling is $\phi_1 = x, -x$; $\phi_2 = x$; $\phi_3 = -x$; $\phi_4 = y$; $\phi_5 = x$; $\phi_6 = x$; $\psi = x$; $\phi_{rec} = x, -x$. In the MQ-HNCO-TROSY scheme (**a**), depending on setting of $0 \le \kappa \le 1$, the position of the downscaled anti-TROSY component varies between ω_N and $\omega_N + \pi J_{NH}$ (*inset* **a′**), whereas in the HR-TROSY HNCO scheme (**b**) with $\kappa \ge 0$, the upscaled anti-TROSY component floats between $\omega_N - \pi J_{NH}$ and $\omega_N - (\kappa + 1)\pi J_{NH}$ (*inset* **b′**). Hence, the measured $(J+D)_{NH}$s are scaled by $(1 + \kappa)/2$ and $\kappa/2$ in the MQ-HNCO-TROSY and HR-TROSY HNCO spectra, respectively. Quadrature detection in the $^{13}C'$ dimension is obtained by States-TPPI protocol applied to ϕ_1 (Marion et al. 1989). For quadrature detection in the indirect ^{15}N dimension, the 90°(^{15}N) with the phase ψ is inverted simultaneously with the gradient G_N to obtain echo/antiecho selection. The data processing is according to the sensitivity enhanced method (Kay et al. 1992). In addition to echo/antiecho coherence transfer pathway selection, the axial peaks are shifted to the edge of the spectrum by inverting ϕ_2 together with ϕ_{rec} in every second t_2 increment

^{15}N–^1H splitting in ^{15}N dimension is less susceptible to additional line broadening due to unresolved ^1H–^1H dipolar couplings even on highly perdeuterated sample. We therefore decided to measure ^{15}N–^1H RDCs in the indirectly detected ^{15}N dimension.

In larger proteins with hundreds of residues, precision of measured ^{15}N–^1H splitting is not solely hampered by the effective linewidth and signal-to-noise ratio (S/N) of the fast decaying ^{15}N magnetization associated with the $^1H^{\beta}$ spin state, the so-called anti-TROSY component, but also by the level of cross peak overlap. Therefore, in case of measurement of $(J + D)_{NH}$s in larger proteins, our aim has been in development of a pulse sequence, which offers a high resolution without sacrificing the sensitivity of experiment. To this end, we utilized an approach based on the accordion spectroscopy (Bodenhausen and Ernst 1981) to determine cross peak position of the upfield ^{15}N-$\{^1H^{\beta}\}$ component. The approach is similar to the implementations proposed by Yang et al. (1999) and Kontaxis et al. (2000), and has been successfully utilized for measuring small $^1D_{NC\alpha}/^2D_{NC\alpha}$ (Permi et al. 2000a; Puttonen et al. 2006) and $^3J_{HNH\alpha}$ couplings (Heikkinen et al. 1999). In this method, additional variable delay κt_2 is incorporated into the pulse sequence during which the coupling interaction between ^1H and ^{15}N is active. In practice, two 180°(^1H) pulses (shown as unfilled rectangular bars in Fig. 1a) are given at the points indicated by A. The $\kappa = 0$ is a special case; the first 180°(^{1}H) pulse does not have any influence on evolution of $(J + D)_{NH}$ Hamiltonian during the experiment. The second 180°(^{1}H) pulse, applied together with the 180°(^{15}N) pulse, decouples any ^{1}H–^{15}N scalar or dipolar coupling interaction during the t_2 period. Afterwards, the TROSY element selects more slowly decaying TROSY component for ^{1}H detection resulting in cross peaks appearing at $\omega_{C'}$, ω_N, and $\omega_{HN} + \pi J_{NH}$ frequencies. Therefore $(J + D)_{NH}$ couplings are measured from the cross peak displacement between the TROSY and the F$_2$-decoupled TROSY ($\kappa = 0$) spectra. Because cross peak positions differ in F$_2$(^{15}N) by πJ_{NH}, the measured splitting is only half of the true coupling, hence doubling the error in measurement.

In case of $0 < \kappa \leq 1$, the first 180°(^{1}H) pulse inverts the ^{1}H spin states and ^{15}N–^{1}H coupling interaction evolves during the κt_2 period, whereas the second 180°(^{1}H) pulse together with 180°(^{15}N) pulse decouples the interaction during t_2. Again, the ensuing TROSY element selects the most slowly relaxing component for ^{1}H detection, resulting in cross peak at $\omega_{C'}$, $\omega_N + \kappa\pi J_{NH}$, and $\omega_{HN} + \pi J_{NH}$ frequencies. Thus, the apparent $(J + D)_{NH}$ is measured between the TROSY and downscaled anti-TROSY spectra, and the frequency of the anti-TROSY component is determined by the factor κ. True couplings are then obtained by multiplying the measured splitting with the factor of $(1 + \kappa)/2$. Using the scaling factor $\kappa = 1$ results in a 'natural' ^{15}N–^{1}H splitting as ^{15}N chemical shift and $(J + D)_{NH}$ coupling evolutions are active for equal periods.

Figure 1b shows a modified, albeit conceptually analogous, implementation of the HR-TROSY HNCO pulse sequence (Hu et al. 2009). Although for recording the TROSY component both experiments are identical, they differ in case of recording the anti-TROSY component. Indeed, when measuring the anti-TROSY component, the signal modulates in the MQ-HNCO-TROSY (Fig. 1a) according to

$$\exp[-(i\omega_N - i\kappa\pi J_{NH})t_2]\exp\left[-\left(-\frac{(1+\kappa)}{2}R_{2T}t_2\right)\right]\exp\left[-\left(\frac{(1+\kappa)}{2}R_{2A}t_2\right)\right] \tag{1}$$

and in the HR-TROSY HNCO (Fig. 1b)

$$\exp[-(i\omega_N + i(1+\kappa)\pi J_{NH})t_2]\exp\left[-\left(\frac{\kappa}{2}R_{2T}t_2\right)\right]\exp\left[-\left(\frac{\kappa}{2}R_{2A}t_2\right)\right] \tag{2}$$

where R_{2T} and R_{2A} correspond to relaxation rates of TROSY and anti-TROSY components, respectively. As we measure the anti-TROSY components with respect to the TROSY cross peak emerging at $\omega_N - \pi J_{NH}$, the required scaling factors are not similar between two experiments and they need to be normalized with respect to MQ-HNCO-TROSY to allow direct comparison of effective relaxation during the pulse sequences. Replacing κ in (2) by $\kappa + 1$ translates into

$$\exp[-(i\omega_N - i(2+\kappa)\pi J_{NH})t_2]\exp\left[-\left(\frac{(1+\kappa)}{2}R_{2T}t_2\right)\right]\exp\left[-\left(\frac{(1+\kappa)}{2}R_{2A}t_2\right)\right] \tag{3}$$

Now, using identical values of κ in (1) and (3) result in identical but opposite offset for the scaled anti-TROSY component from the TROSY cross peak. In this case, the relevant relaxation exponents for MQ-HNCO-TROSY and HR-TROSY HNCO then become

$$\exp\left[-\left((R_{2A} - R_{2T})\frac{1}{2}(1+\kappa)t_2\right)\right] \tag{4}$$

and

$$\exp\left[-\left((R_{2A} + R_{2T})\frac{1}{2}(1+\kappa)t_2\right)\right], \tag{5}$$

respectively. Hence, the effective relaxation rates for the scaled anti-TROSY components in the MQ-HNCO-TROSY and HR-TROSY HNCO experiments are $1/2 \times (1+\kappa) \times (R_{2A} - R_{2T})$ and $1/2 \times (1+\kappa) \times (R_{2A} + R_{2T})$, respectively. Line narrowing can be observed by comparing relaxation exponents between the MQ-HNCO-TROSY and HR-TROSY HNCO experiments. As linewidth is a function of effective relaxation rate, we can directly observe:

$$\frac{LW_{MQ-HNCO-TROSY}}{LW_{HR-TROSY-HNCO}} = \exp[-(1+\kappa)R_{2T}t_2] < 1 \tag{6}$$

where $\kappa \geq 0$ and LW is peak linewidth. For instance, using the factor $\kappa = 1$, i.e. no scaling of the apparent $(J + D)_{NH}$ splitting, results in additional line broadening in the HR-TROSY HNCO scheme by $\exp[2R_{2T}t_2]$ Despite the 2–7 times larger R_{2A} in comparison to R_{2T}, the additional line broadening is far from being negligible even on perdeuterated 60 kDa system.

Figure 2 shows 1D traces along ^{15}N dimension from K10–A34 residues in small 56-residue protein GB1. Overlays of the TROSY component (middle) and downscaled and upscaled anti-TROSY components of the MQ-HNCO-TROSY (right) and HR-TROSY HNCO (left) spectra, recorded with different κ values are shown for K10 (Fig. 2a) and A34 (Fig. 2b). It can be observed that the apparent frequency difference and linewidth increase, whereas the sensitivity decreases, with increasing κ. In case of $\kappa = 0$, the line broadening for the upfield (downscaled anti-TROSY line) multiplet component is counterbalanced by refocused long-range coupling interactions between ^{15}N and ^{1}H during the t_2 in non-deuterated sample. Two- and three-bond couplings between

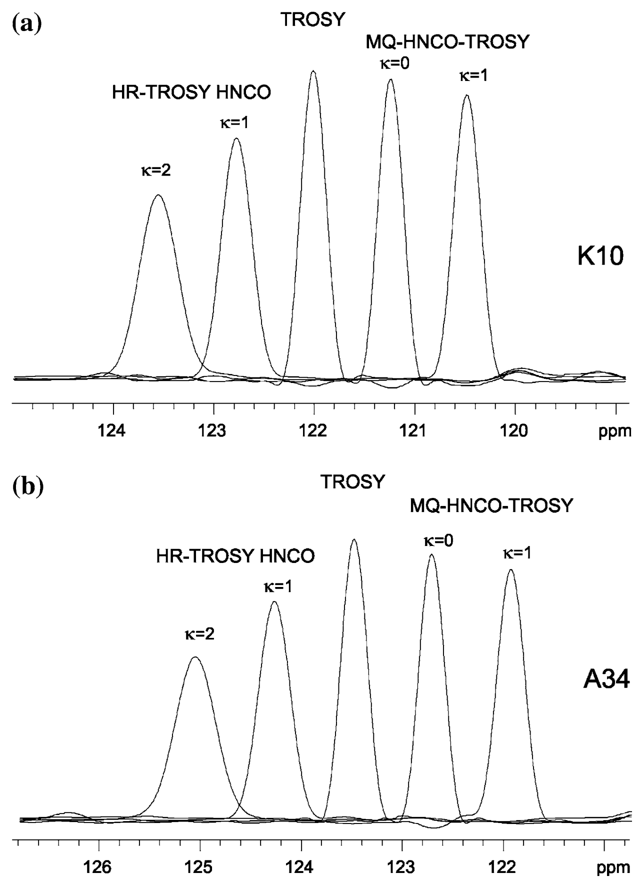

Fig. 2 Expansions of K10 (**a**) and A34 (**b**) cross peaks from GB1 along the ^{15}N dimensions. For both residues, four spectra with the anti-TROSY components and a spectrum with the TROSY component are overlaid. The TROSY component was recorded for the reference, using the MQ-HNCO-TROSY experiment, and is shown in the middle. Two upscaled anti-TROSY spectra (*left*) were recorded with $\kappa = 1$ and $\kappa = 2$ using the modified HR-TROSY HNCO experiment. Two spectra on the *right* show the downscaled anti-TROSY components, which were recorded with scaling factors $\kappa = 0$ and $\kappa = 1$ using the MQ-HNCO-TROSY pulse sequence

^{15}N(i) and ^{1}H$^{\alpha}$(i), and ^{1}H$^{\alpha}$($i - 1$) range typically from -0.5 to -2 Hz and 0.1 to -2 Hz (Permi et al. 2000b; Permi 2003; Wang and Bax 1995), whereas three-bond scalar couplings up to 5–6 Hz between ^{15}N(i) and ^{1}H$^{\beta}$(i) have been reported (Düx et al. 1999). In case of $\kappa = 1$, the apparent linewidth is 10 and 13% larger in comparison to decoupled ^{15}N component with $\kappa = 0$ for K10 and A34, respectively. This line broadening is due to faster decay of ^{15}N transverse magnetization (anti-TROSY effect) during $\kappa t_2/2$ as well as contribution of long-range ^{15}N–^{1}H couplings to the effective line width. In contrast, the line width in HR-TROSY HNCO spectrum increases by 52% for K10 and 47% for A34 when using the scaling factor $\kappa = 2$ instead of $\kappa = 1$. Comparison of attainable line widths between the MQ-HNCO-TROSY (Fig. 1a) and HR-TROSY HNCO (Fig. 1b) schemes reveals significant differences. As demonstrated for A34 and K10 in Fig. 2, the apparent line width obtained with the MQ-HNCO-TROSY scheme is significantly smaller in comparison to the HR-TROSY HNCO method (Fig. 1b), where the spin-echo period follows the chemical shift labeling period. Indeed, line width is nearly 50% larger in HR-TROSY HNCO ($\kappa = 2$) spectrum in comparison to the corresponding MQ-HNCO-TROSY ($\kappa = 1$) spectrum. This is mainly governed by additional signal decay during the κt_2 period, which is implemented in a constant-time manner in Fig. 1a instead of a real-time implementation shown in Fig. 1b.

In order to verify accuracy of these approaches in practice, we measured $^{1}J_{NH}$s in ^{15}N/^{13}C labeled human ubiquitin (76 residues, MW 8.6 kDa) using the MQ-HNCO-TROSY experiment with two different κ values ($\kappa = 0$ and $\kappa = 1$) and compared them with the reference values obtained using the generalized 2D ^{15}N, ^{1}H TROSY experiment (Andersson et al. 1998; Weigelt 1998). A pair-wise comparison of $^{1}J_{NH}$s obtained using the proposed approach to the reference values measured using the 2D TROSY experiment, gave a Pearson correlation of $R = 0.94$ and $R = 0.95$ with an RMSD of 0.30 Hz and 0.26 Hz for $\kappa = 0$ and $\kappa = 1$, respectively. Correlation plots between the proposed method and the reference experiment shown in Fig. 3 reveal no obvious systematic errors, suggesting that $^{1}J_{NH}$s can be measured with a sufficient accuracy by the proposed methodology, and the attainable precision is mainly governed by the apparent line width and sensitivity.

The precision by which the cross peak placement can be determined is according to Bax et al. (2001) defined by:

$$\Delta J = \frac{\mathrm{LW}}{\mathrm{SN}} \qquad (7)$$

where ΔJ is a crude estimation of the attainable precision (RMSD) of a coupling in Hz, LW is the attainable signal line width at the half height in Hz, and SN is the signal-to-noise ratio of the peak.

Accurate determination of couplings with the proposed MQ-HNCO-TROSY scheme depends also on the scaling factor κ, which also scales the random error. Although it seems convenient to perform measurements with $\kappa = 1$, in which case no scaling is required, smaller κ improves the overall sensitivity and decrease the apparent line width. Hence, the precision of measured couplings is a trade-off between LW/SN and the scaling of the random error. Determination of J coupling with $\kappa = 1$ leads to precision $\Delta J_{\kappa=1} = \mathrm{LW}_1/\mathrm{SN}_1$ whereas the same coupling can be measured, for instance with $\kappa = 0$ and multiplying the result by factor of 2, thus leading to precision $\Delta J_{\kappa=0} = 2 \times \mathrm{LW}_0/\mathrm{SN}_0$. To a first approximation, precision follows coarse relation

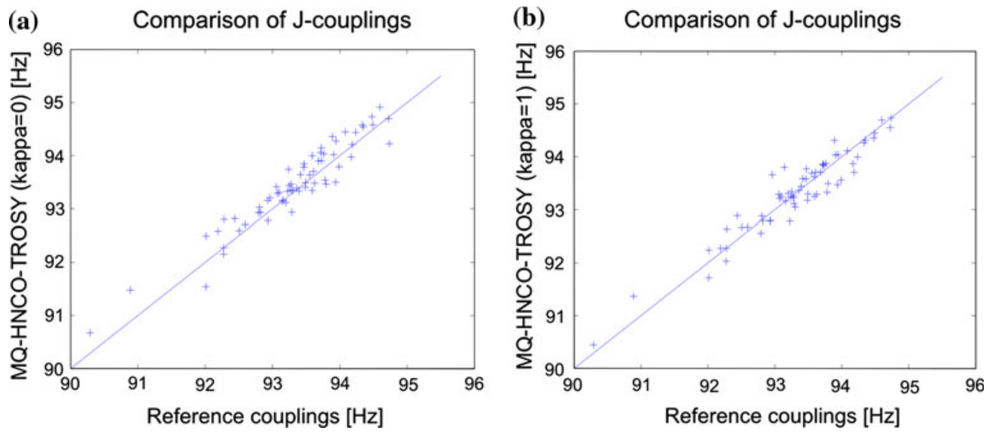

Fig. 3 Correlations between scalar ${}^{1}J_{NH}$ couplings obtained using the reference experiment (Andersson et al. 1998; Weigelt 1998) and the MQ-HNCO-TROSY pulse sequence. Pearson's correlations for (**a**) and (**b**) are $R = 0.94$ and $R = 0.95$ with RMSD of 0.30 and 0.26 Hz, respectively. MQ-HNCO-TROSY spectra were collected using the scaling factors $\kappa = 0$ and $\kappa = 1$ for data in (**a**) and (**b**)

$$\Delta J_i = \frac{\mathrm{LW}_i}{\mathrm{SN}_i} = \frac{(\kappa_j + 1)}{(\kappa_i + 1)} \times \frac{\mathrm{LW}_j}{\mathrm{SN}_j} = \frac{(\kappa_j + 1)}{(\kappa_i + 1)} \times \Delta J_j \qquad (8)$$

where i and j refer to affiliated κ values. It is noteworthy that this description does not take into account line narrowing or signal to noise enhancement with smaller κ values. Although more sophisticated correction factors can be applied for determining LW/SN with different κ values, we preferred determination of LW/SN experimentally. As shown in recent studies, methods with the downscaled couplings provide higher precision for fast decaying signal on larger proteins (Kontaxis et al. 2000; Tugarinov and Kay 2003). As noted by Bax et al. (2001), the ΔJ defines only the lower limit of precision, while several other factors, most prominently resonance overlap, hamper the accurate determination of the splitting. These conditions are often met in the case of larger proteins, where both extensive cross peak overlap and prohibitively fast relaxation of the anti-TROSY component governs the attainable accuracy and precision of measured $(J + D)_{NH}$s.

We measured MQ-HNCO-TROSY experiment with different κ values on larger monomeric protein, a 60-kDa fragment (557 residues) of filamin A, and compared line-widths and resolution of obtained spectra. Structural arrangement of filamin A is modular, comprised of six adjacent filamin-type immunoglobulin-like domains 16–21 (IgFLNa16–21), with average ^{15}N transverse relaxation rates of 30–40 s^{-1}, that make IgFLNa16–21 a highly challenging molecular system to be studied by solution state NMR spectroscopy. Although perdeuteration was a pre-requisite for the measurement of RDCs in this high molecular weight system, increased resonance overlap due to large monomeric architecture generates an additional challenge. MQ-HNCO-TROSY experiment provided adequate resolution in the ^{15}N dimension and enabled measurement of 84% of all possible $(J + D)_{NH}$s in IgFLNa16–21 Resolution enhancement in the ^{15}N dimension, obtained using the novel scheme instead of the conventional HNCO is illustrated in Fig. 4. Clearly the separation of cross peaks (the TROSY component) in the ^{15}N dimension is significantly better in the MQ-HNCO-TROSY spectrum (Fig. 4a) than in the conventional HNCO-TROSY spectrum (Fig. 4b).

Fast relaxation of the anti-TROSY component establishes an additional problem in large proteins such as IgFLNa16–21. Figure 5a shows expansions of 1D ^{15}N traces taken through K1824, Y1862 and H2061 cross peaks of ^{15}N, ^{13}C, ^{2}H labeled IgFLNa16–21. Again shown are the TROSY spectrum (in the middle) overlaid with the anti-TROSY spectra recorded using the MQ-HNCO-TROSY experiment with $\kappa = 0$ and $\kappa = 1$ (right) and HR-TROSY HNCO experiment with $\kappa = 1$ and $\kappa = 2$ (left). It is clearly evident from Fig. 5a that linewidth of the upfield ^{15}N-{^{1}H} component increases rapidly with increasing κ. For instance, in case of MQ-HNCO-TROSY experiment with $\kappa = 0$, the non-apodized linewidth and S/N ratio for the downscaled anti-TROSY component of K1824 are 14.2 Hz and 22.2, whereas they are 16.7 Hz and 17.4 with $\kappa = 1$, respectively. However, in the HR-TROSY HNCO spectrum, the corresponding line widths for the upscaled anti-TROSY component are 16.9 Hz ($\kappa = 1$) and 23.8 Hz ($\kappa = 2$). A similar trend is observed also in the cases of Y1862 and H2061. Although line broadening is less dramatic when compared to non-deuterated GB1 (Fig. 2) due to greater R_{2A}/R_{2T} ratio in the perdeuterated sample, this indicates that contribution of slowly decaying (R_{2T}) magnetization to the overall linewidth of broad multiplet component is not negligible even on large perdeuterated protein. Attainable linewidths for 25 well-resolved ^{15}N–^{1}H cross peaks in ^{15}N, ^{13}C, ^{2}H labeled IgFLNa16–21 are presented in Fig. 5b, showing that linewidths acquired with HR-TROSY HNCO are larger than those recorded with MQ-HNCO-TROSY experiment.

It can be anticipated that performance of the proposed MQ-HNCO-TROSY experiment sustains superiority to HR-TROSY HNCO despite the fact that the ratio R_{2A}/R_{2T} increases as polarizing magnetic field, B_0, approaches the

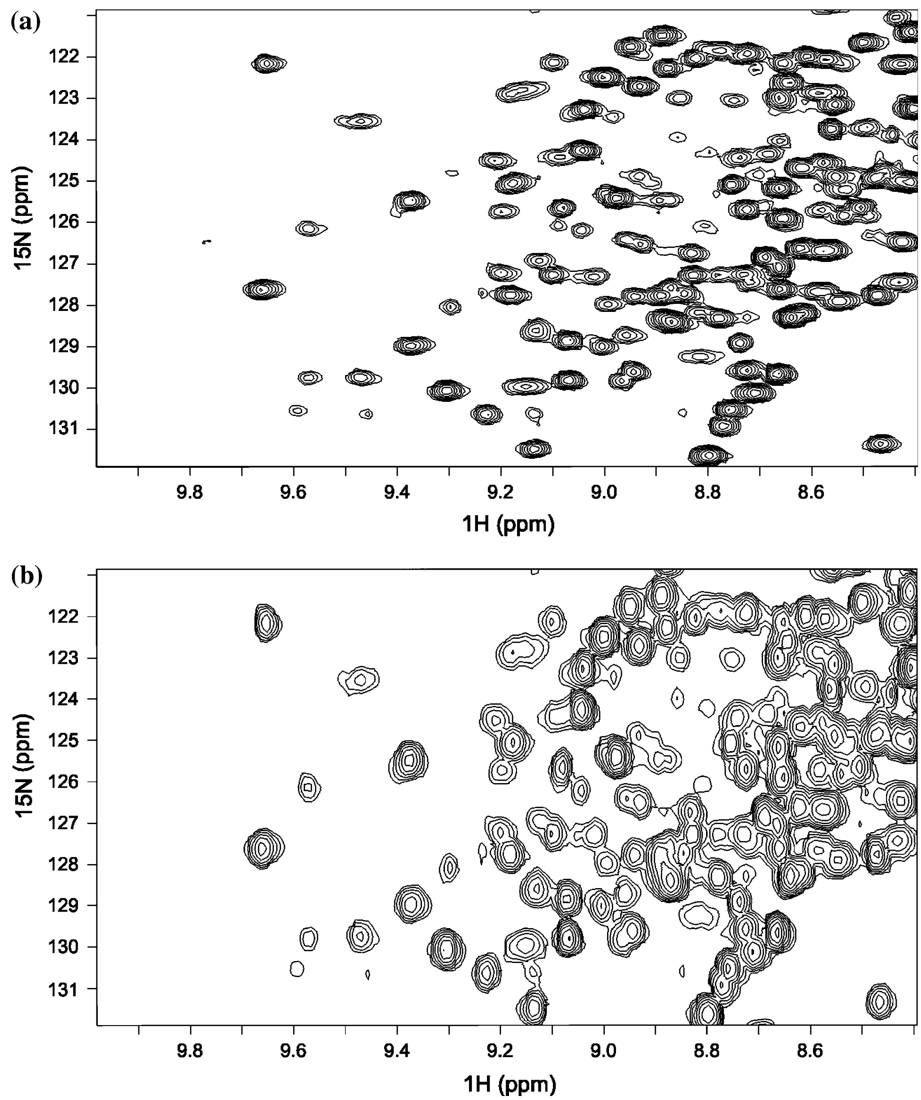

Fig. 4 Representative expansion of two-dimensional ^{15}N–^{1}H MQ-HNCO-TROSY spectrum from IgFLNa16–21. Spectrum in the panel (**a**), showing the TROSY components, was recorded using 118 complex points in ^{15}N dimension ($t_{2,\max} \sim 47.2$ ms) and the spectrum in the panel (**b**)—with 59 complex points in t_2 ($t_{2,\max} \sim 23.6$ ms)

optimal 900–1,000 MHz field strength, where the ^{15}N chemical shift anisotropy (CSA) and ^{15}N–^{1}H dipolar coupling (DD) relaxation mechanisms cancel each other (Pervushin et al. 1997). Several ^{15}N–^{1}H spin moieties are influenced by additional relaxation mechanisms violating optimal TROSY conditions e.g. chemical exchange contribution or a slight variation in the magnitude or orientation of the ^{15}N CSA tensor between residues in α-helix and β-sheet. Therefore, contribution of R_{2T} during κt_2 period to the overall linewidth is non-zero.

Further inspection of attainable linewidths reveals that in case of larger proteins, the most advantageous strategy to determine $^{1}(D + J)_{NH}$s is to measure the corresponding splitting symmetrically around the TROSY component as reported by Tolman and co-workers (Abrogast et al. 2010). To that end, schemes in Fig. 1a and b are combined to measure downscaled and up-scaled anti-TROSY components with scaling factors $\kappa = 0$ and $\kappa = 1$, respectively. This results in two cross peaks emerging at $\omega_{C'}$, ω_N, $\omega_{HN} + \pi J_{NH}$ and $\omega_{C'}$, $\omega_N - 2\pi J_{NH}$, $\omega_{HN} + \pi J_{NH}$ frequencies. Therefore, $^{1}(D + J)_{NH}$s can be obtained between two anti-TROSY cross peaks offset from the TROSY transition by $\pm\pi J_{NH}$, which provides optimal sensitivity and resolution in case of larger proteins (Abrogast et al. 2010).

Using the scaling factor $\kappa = 1$ instead of $\kappa = 0$ for measuring the anti-TROSY component provided higher accuracy in case of K1824 in IgFLNa16–21, with Δ*J*s of 0.96 and 1.28 Hz, respectively. However, we decided to use the scaling factor $\kappa = 0$, resulting in the apparent $(J + D)_{NH}/2$ splitting, as transverse relaxation of an anti-TROSY component for several residues is significantly faster than we found for K1824. Hence, we employed the proposed MQ-HNCO-TROSY experiment at 800 MHz for measuring ^{15}N–^{1}H RDCs in IgFLNa16–21 from the cross peak displacement between the TROSY and downscaled

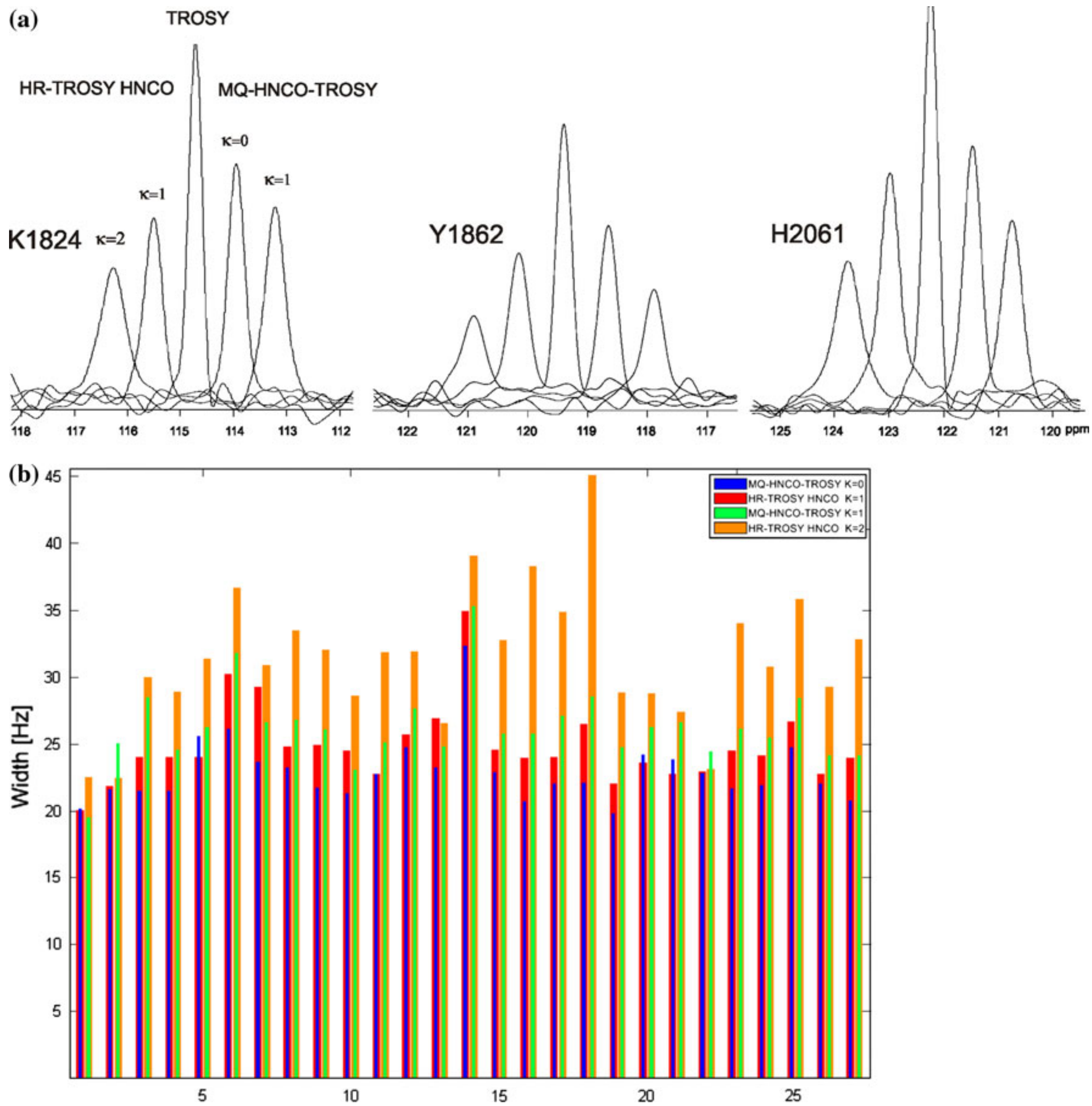

Fig. 5 **a** Representative expansions along the ^{15}N dimension from the two-dimensional ^{15}N–^{1}H MQ-HNCO-TROSY spectrum of ^{2}H, ^{13}C, ^{15}N labeled IgFLNa16–21. Excerpts are taken through the cross peaks of residues K1824, Y1862, and H2061. TROSY and down-scaled anti-TROSY ($\kappa = 0$ and $\kappa = 1$) components, recorded with the MQ-HNCO-TROSY scheme, and upscaled anti-TROSY ($\kappa = 1$ and $\kappa = 2$) components, recorded with the HR-TROSY HNCO pulse scheme, are shown overlaid. **b** Linewidths for 25 well-resolved ^{15}N–^{1}H cross peaks in MQ-HNCO-TROSY and HR-TROSY HNCO spectra. *Blue* and *green bars* show apparent line widths obtained using the MQ-HNCO-TROSY experiment with $\kappa = 0$ and $\kappa = 1$, respectively. The bars corresponding to values obtained with the HR-TROSY HNCO experiment with $\kappa = 1$ and $\kappa = 2$ are highlighted with *red* and *orange* colors, respectively

anti-TROSY components, recorded with the scheme in Fig. 1a using the scaling factor $\kappa = 0$. RDCs were extracted from the difference between ^{15}N–^{1}H splittings measured in water and in a diluted liquid crystal medium composed of filamentous phage Pf1 particles (Hansen et al. 1998) as demonstrated for K1824, T1984 and G2008 in Fig. 6a and b. In total, we measured 431 RDCs, spanning from −60 to 50 Hz. Degree of alignment varied quite substantially between individual domains of IgFLNa16–21. D_{max} of ~20–30 Hz was found for domains 16–19, whereas couplings as large as −60 Hz were measured for domains 20–21. We compared the experimentally determined RDCs from IgFLNa16–21 to those predicted from the existing NMR (IgFLNa16–17 and IgFLNa18–19) and crystal (IgFLNa19–21) structures (Heikkinen et al. 2009; Lad et al. 2007), using singular value decomposition algorithm (Losonczi et al. 1999) implemented into the software package PALES (Zweckstetter and Bax 2000). A pair-wise comparison of the calculated RDCs, based on the NMR structure of IgFLNa16–17 (PDB ID: 2K7P), to corresponding experimental couplings from domains 16 to 17 in IgFLNa16–21 yield Q-factor 0.34 (Fig. 7a), indicating

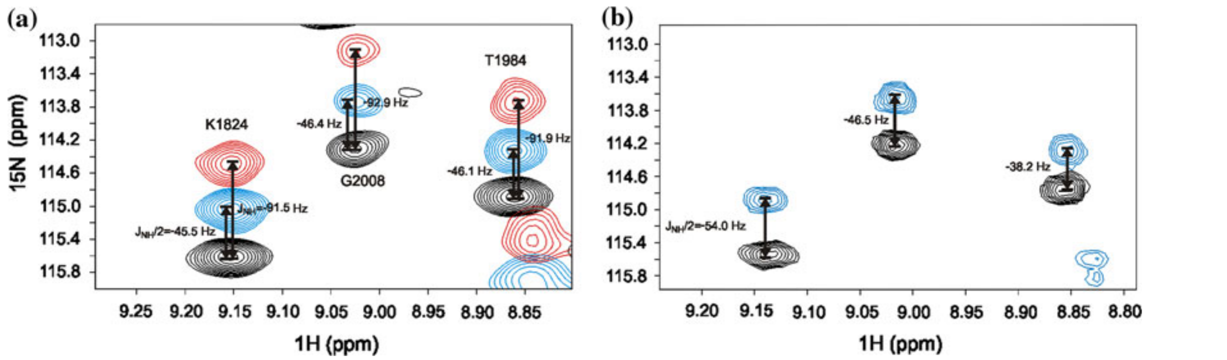

Fig. 6 Two-dimensional expansions of K1824, T1984 and G2008 cross peaks in water (**a**) and in phage (**b**). TROSY components are shown with *black* contour, downscaled anti-TROSY ($\kappa = 0$) with blue contours and downscaled anti-TROSY ($\kappa = 1$) with *red* contours. The measured splittings in water between the TROSY and anti-TROSY ($\kappa = 0$), and TROSY and anti-TROSY ($\kappa = 1$) are highlighted in the panel (**a**) The corresponding splittings (in phage) between the TROSY and anti-TROSY ($\kappa = 0$) components are shown in the panel (**b**)

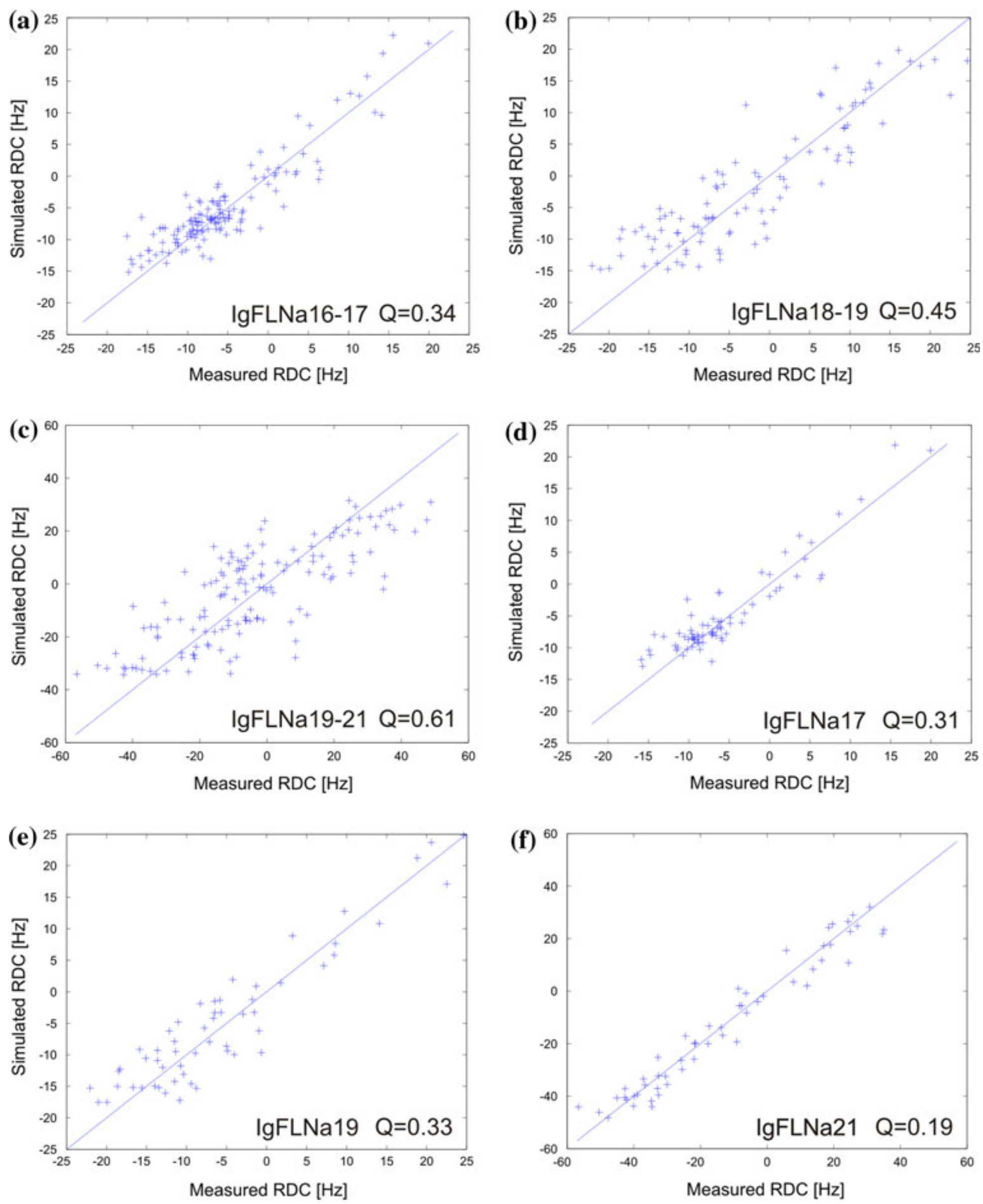

Fig. 7 Correlations between the experimental $^{1}D_{NH}$s and the predicted couplings calculated from **a** IgFLNa16–17 NMR structure, **b** IgFLNa18–19 NMR structure, and **c** IgFLNa19–21 crystal structure. **d** A pair-wise comparison of experimental and the predicted $^{1}D_{NH}$ values of the domain 17 from IgFLNa16–17, **e** the domain 19 from IgFLNa18–19, and the domain 21 from IgFLNa19–21. The fits were obtained by using the singular value decomposition method (Losonczi et al. 1999) integrated into the program PALES (Zweckstetter and Bax 2000)

good fit between experimental RDCs and NMR coordinates based on NOE restraints (Heikkinen et al. 2009). In contrast to the domain pair 16–17, the fits between predicted and experimental RDCs for domain pair 18–19 (PDB ID: 2K7Q) as well as for the crystal structure of IgFLNa19–21 (PDB ID: 2J3S) gave significantly worse correlations with Q-factors of 0.45, and 0.61, respectively (Fig. 7b, c). We take this as an indication of significant differences in domain orientations between isolated domain pairs rather than insufficient quality of experimental RDC data because the dynamic range of RDCs measured from IgFLNa16–21 is several-fold larger than contribution of random error, which we estimate to be ±(2–3) Hz for the measured RDC. Experimental RDCs measured from IgFLNa16–21 clearly correlate better with the back-calculated values from the individual domains of IgFLNa16–17, IgFLNa18–19 and IgFLNa19–21 structures, resulting in Q-factors of 0.33, 0.31, 0.38, 0.33, 0.24, and 0.19, respectively (Fig. 7d–f). In these cases, a total of 321 RDCs were utilized for fittings. RDCs of the residues residing at domain boundaries or showing elevated internal mobility, or which were missing in the crystal structure (residues 2,163–2,170 and 2,191–2,197) were not included to the fits. We reckon that the poor fit between experimental and back-calculated RDCs originate either from the difference between isolated domains (IgFLNa18–19 and IgFLNa19–21) and larger molecular construct (IgFLNa16–21) or the difference between solution and crystal lattices of IgFLNa19–21.

Conclusions

We have introduced a modified HNCO-TROSY pulse sequence for measuring scalar and residual dipolar couplings in large proteins. The proposed MQ-HNCO-TROSY experiment suits well for measuring RDCs in high molecular weight systems with large number of cross peaks. This advantage can be attributed to two main reasons: the experiment provides a significantly higher resolution in ^{15}N dimension with respect to the traditional HNCO-TROSY, thus diminishing cross peak overlap, and minimizes the time period during which the ^{15}N spin is susceptible to fast transverse relaxation associated with the anti-TROSY transition. In the proposed scheme, the whole $2T_N$ period is used for labeling of ^{15}N chemical shift in a constant time manner, which efficiently doubles the attainable resolution in ^{15}N dimension with respect to the conventional HNCO-TROSY experiment. We employed the MQ-HNCO-TROSY scheme with $\kappa = 0$ for measuring RDCs in high molecular weight protein IgFLNa16–21 with 557 residues, resulting in 431 RDCs. Correlations between experimental and back-calculated RDCs in individual domains gave relatively low value Q factors, indicative of sufficient accuracy that can be obtained with the proposed MQ-HNCO-TROSY experiment in high molecular weight proteins. We believe that the proposed MQ-HNCO-TROSY experiment will be very useful for measuring $^1D_{NH}$s in larger proteins.

Experimental

The MQ-HNCO-TROSY pulse sequence for measuring scalar couplings was tested on three proteins: 1.9 mM uniformly ^{15}N/^{13}C labeled human ubiquitin (8.6 kDa, 76 residues) in10 mM Na-PO_4, pH 5.8, supplemented with 5% (v/v) D_2O. 1.5 mM uniformly ^{15}N, ^{13}C labeled immunoglobulin-binding domain B1 of streptococcal protein G (GB1, 6.5 kDa, 56 residues) in 20 mM Na-PO_4, pH 5.5, supplemented with 7.5% (v/v) D_2O, and 0.5 mM uniformly ^{15}N, ^{13}C, ^{2}H labeled IgFLNa16–21 (60 kDa, 557 residues) in 50 mM Na-PO_4, pH 6.8, 100 mM NaCl, 1 mM DTT and 2 mM NaN, supplemented with 7% (v/v) D_2O. In order to measure residual dipolar couplings, ^{15}N, ^{13}C, ^{2}H labeled IgFLNa16–21 was dissolved in a dilute liquid crystal medium, composed of filamentous phage particles, Pf1. The phage concentration was 15 mg/ml and the final protein concentration was 0.4 mM.

Spectra for ubiquitin and GB1 were acquired on a Varian Unity INOVA 800 and 600 MHz NMR spectrometers, respectively. Spectra for IgFLNa16-21 were measured on a Varian Unity INOVA 600 and 800 MHz NMR spectrometers. Spectrometers were equipped with a ^{1}H/^{13}C/^{15}N triple-resonance probeheads and actively shielded *Z*-axis gradient systems. Spectra were processed using the standard VNMRJ 2.1 revision B software package (Varian associates, 2006), and analyzed with VNMRJ2.1 and Sparky 3.110 (Goddard and Kneller, 2004). All spectra for ubiquitin and GB1 were measured at 25°C and at 30°C for IgFLNa16-21.

In case of GB1, the two-dimensional MQ-HNCO-TROSY (HR-TROSY HNCO) spectra with values of $\kappa = 0$ and $\kappa = 1$ ($\kappa = 1$ and $\kappa = 2$) were recorded using 2 transients per FID with 128 and 512 complex points, corresponding to acquisition times of 62 and 51.2 ms in ^{15}N and ^{1}H dimensions, respectively. Experimental time per each spectrum was 16 min. For each spectrum, prior to zero-filling to 4,096 × 4,096 data matrix and Fourier transform, identical shifted squared sine-bell weighting function were applied to both dimensions.

In case of ubiquitin, the two-dimensional MQ-HNCO-TROSY spectra, recorded with the pulse sequence shown in Fig. 1a using the $\kappa = 0$ and $\kappa = 1$ values, and the generalized 2D ^{15}N, ^{1}H TROSY experiment (Andersson et al. 1998; Weigelt 1998) were employed. Spectra were acquired with 2 transients per FID with 128 and 853 complex points in ^{15}N and ^{1}H dimensions, respectively. These correspond to acquisition times of 62 and 85.3 ms in t_1 and t_2, respectively. For each spectrum, prior to zero-filling to 4,096 × 4,096 data matrix and Fourier transform, identical shifted squared sine-bell weighting functions were applied to both dimensions.

For comparison of attainable line widths in IgFLNa16-21 at 600 MHz, two-dimensional ^{15}N, ^{1}H correlation spectra with $\kappa = 0$ (Fig. 1a), $\kappa = 1$ (Fig. 1a, b) and $\kappa = 2$ (Fig. 1b) were acquired using 48 transients per FID with 120 and 853 complex points, corresponding to acquisition times of 60.0 and 85.3 ms in ^{15}N and ^{1}H dimensions, respectively. Total experimental time was 5 h for each spectrum. For each spectrum, prior to zero-filling to 4,096 × 4,096 data matrix and Fourier transform, identical shifted squared sine-bell weighting function were applied to both dimensions.

Three-dimensional MQ-HNCO-TROSY spectrum (in water/phage) was acquired using 2 transients per FID with 32, 128 and 853 complex points, corresponding to acquisition times of 18.2, 49.2, and 85.3 ms in t_1(^{13}C′), t_2(^{15}N), and t_3(^{1}H), respectively. Interscan delays were 1.55/2.4 s for the sample in water/phage, respectively. Shifted squared sine-bell weighting functions were applied to all three dimensions before zero-filling to 256 × 1,024 × 2,048 data matrix and Fourier transform. TROSY and downscaled anti-TROSY components were measured in an interleaved manner and the scaling factor $\kappa = 0$ was used. Total acquisition time was 79 and 118 h for spectrum recorded in water and phage, respectively.

References

Abrogast L, Majumdar A, Tolman JR (2010) HNCO-based measurement of one-bond amide ^{15}N–^{1}H couplings with optimized precision. J Biomol NMR 46:175–189

Andersson P, Annila A, Otting G (1998) An α/β-HSQC-α/β experiment for spin-state selective editing of IS cross peaks. J Magn Reson 133:364–367

Annila A, Permi P (2004) Weakly aligned biological macromolecules in dilute aqueous liquid crystals. Concepts Magn Reson 23A:22–37

Bax A, Kontaxis G, Tjandra N (2001) Dipolar couplings in macromolecular structure determination. Methods Enzymol 339:127–174

Blackledge M (2005) Recent progress in the study of biomolecular structure and dynamics in solution from residual dipolar couplings. Prog Nucl Magn Reson Spectr 46:23–61

Bodenhausen G, Ernst RR (1981) The accordion experiment, a simple approach to 3-dimensional NMR spectroscopy. J Magn Reson 45:367–373

Bouvignies G, Markwick PRL, Blackledge M (2007) Simultaneous definition of high resolution protein structure and backbone conformational dynamics using NMR residual dipolar couplings. ChemPhysChem 8:1901–1909

Düx P, Whitehead B, Boelens R, Kaptein R, Vuister GW (1999) Measurement of ^{15}N–^{1}H coupling constants in uniformly ^{15}N-labeled proteins: application to the photoactive yellow protein. J Biomol NMR 10:301–306

Fischer MW, Losonczi JA, Weaver JL, Prestegard JH (1999) Domain orientation and dynamics in multidomain protein from residual dipolar couplings. Biochemistry 38:9013–9022

Fredriksson K, Louhivuori M, Permi P, Annila A (2004) On the interpretation of residual dipolar couplings as reporters of molecular dynamics. J Am Chem Soc 126:12646–12650

Hansen MR, Mueller L, Pardi A (1998) Tunable alignment of macromolecules by filamentous phage yields dipolar coupling interactions. Nat Struct Biol 5:1065–1074

Heikkinen S, Aitio H, Permi P, Folmer R, Lappalainen K, Kilpeläinen I (1999) J-multiplied HSQC (MJ-HSQC): a new method for measuring ^{3}J(HNHα) couplings in ^{15}N-labeled proteins. J Magn Reson 137:243–246

Heikkinen OK, Ruskamo S, Konarev PV, Svergun DI, Iivanainen T, Heikkinen SM, Permi P, Koskela H, Kilpeläinen I, Ylänne J (2009) Atomic structures of two novel immunoglobulin-like domain pairs in the actin cross-linking protein filamin. J Biol Chem 284:25450–25458

Hu K, Doucleff M, Clore GM (2009) Using multiple quantum-coherence to increase the ^{15}N resolution in a three-dimensional TROSY-HNCO experiment for accurate PRE and RDC measurements. J Magn Reson 200:173–177

Kay LE, Keifer P, Saarinen T (1992) Pure absorption gradient-enhanced heteronuclear single-quantum correlation spectroscopy with improved sensitivity. J Am Chem Soc 114:10663–10665

Kontaxis G, Clore GM, Bax A (2000) Evaluation of cross-correlation effects and measurement of one-bond couplings in proteins with short transverse relaxation times. J Magn Reson 143:184–196

Lad Y, Kiema T, Jiang P, Pentikäinen O, Coles CH, Campbell ID, Calderwood DA, Ylänne J (2007) Structure of three tandem filamin domains reveals auto-inhibition of ligand binding. EMBO J 26:3993–4004

Lakomek NA, Carlomagno T, Becker S, Griesinger C, Meiler J (2006) A thorough dynamic interpretation of residual dipolar couplings in ubiquitin. J Biomol NMR 34:101–115

Lerche MH, Meissner A, Poulsen FM, Sørensen OW (1999) Pulse sequences for measurement of one-bond (15)N-(1)H coupling constants in the protein backbone. J Magn Reson 140:259–263

Losonczi JA, Andrec M, Fischer MWF, Prestegard JH (1999) Order matrix analysis of residual dipolar couplings using singular-value decomposition. J Magn Reson 138:334–342

Madsen JC, Sørensen OW, Sørensen P, Poulsen FM (1993) Improved pulse sequences for measuring coupling constants in ^{13}C, ^{15}N-labeled proteins. J Biomol NMR 3:239–244

Marion D, Ikura M, Tschudin R, Bax A (1989) Rapid recording of 2D NMR-spectra without phase cycling—application to the study of hydrogen-exchange in proteins. J Magn Reson 85:393–399

McCoy MA, Mueller L (1992) Selective shaped pulse decoupling in NMR: homonuclear [^{13}C]carbonyl decoupling. J Am Chem Soc 114:2108–2112

Meissner A, Duus JO, Sørensen OW (1997) Integration of spin-state-selective excitation into 2D NMR correlation experiments with the heteronuclear ZQ/DQ π rotations for $^{1}J_{XH}$-resolved E.COSY-type measurement of heteronuclear coupling constants in proteins. J Biomol NMR 10:89–94

Nietlispach D (2005) Suppression of anti-TROSY lines in a sensitivity-enhanced gradient selection TROSY scheme. J Biomol NMR 31:161–166

Ottiger M, Delaglio F, Bax A (1998) Measurement of *J* and dipolar couplings from simplified two-dimensional NMR spectra. J Magn Reson 131:373–378

Pääkkönen K, Sorsa T, Drakenberg T, Pollesello P, Tilgmann C, Permi P, Heikkinen S, Kilpeläinen I, Annila A (2000) Conformations of the regulatory domain of cardiac troponin C examined by residual dipolar couplings. Eur J Biochem 267: 6665–6672

Permi P (2002) A spin-state-selective experiment for measuring heteronuclear one-bond and homonuclear two-bond couplings from an HSQC-type spectrum. J Biomol NMR 22:27–35

Permi P (2003) Measurement of residual dipolar couplings from $^{1}H^{\alpha}$ to $^{13}C^{\alpha}$ and ^{15}N using a simple HNCA-based experiment. J Biomol NMR 27:341–349

Permi P, Rosevear PR, Annila A (2000a) A set of HNCO-based experiments for measurement of residual dipolar couplings in ^{15}N, ^{13}C, (^{2}H) labeled proteins. J Biomol NMR 17:43–54

Permi P, Kilpeläinen I, Annila A (2000b) Determination of backbone angle ψ in proteins using a TROSY-based α/β-HN(CO)CA-J experiment. J Magn Reson 146:255–259

Pervushin K, Billeter M, Siegal G, Wüthrich K (1997) Attenuated T_2 relaxation by mutual cancellation of dipole–dipole coupling and chemical shift anisotropy indicates an avenue to NMR structures very large biological macromolecules in solution. Proc Natl Acad Sci U S A 94:12366–12371

Prestegard JH, Al-Hashimi HM, Tolman JR (2000) NMR structures of biomolecules using field oriented media and residual dipolar couplings. Quart Rev Biophys 33:371–424

Puttonen E, Tossavainen H, Permi P (2006) Simultaneous determination of one- and two-bond scalar and residual dipolar couplings between $^{13}C'$, $^{13}C^{\alpha}$, and ^{15}N spins in proteins. Magn Reson Chem 44:168–176

Salzmann M, Pervushin K, Wider G, Senn H, Wüthrich K (1998) TROSY in triple-resonance experiments: new perspectives for sequential NMR assignment of large proteins. Proc Natl Acad Sci U S A 95:13585–13590

Tjandra N, Bax A (1997) Direct measurement of distances and angles in biomolecules by NMR in a dilute liquid crystalline medium. Science 278:1111–1114

Tolman JR, Ruan K (2006) NMR residual dipolar couplings as probes of biomolecular dynamics. Chem Rev 106:1720–1736

Tugarinov V, Kay LE (2003) Quantitative NMR studies of high molecular weight proteins: application to domain orientation and ligand binding in the 723 residue enzyme malate synthase G. J Mol Biol 327:1121–1133

Wang AC, Bax A (1995) Reparametrization of the Karplus relation for $^{3}J(H^{\alpha}$-N) and $^{3}J(H^{N}$-C′) in peptides from uniformly $^{13}C/^{15}N$-enriched human ubiquitin. J Am Chem Soc 117:1810–1813

Weigelt J (1998) Single scan, sensitivity- and gradient-enhanced TROSY for multidimensional NMR experiments. J Am Chem Soc 120:10778–10779

Yang DW, Kay LE (1999) Improved ^{1}HN-detected triple resonance TROSY-based experiments. J Biomol NMR 13:3–10

Yang DW, Venters RA, Mueller GA, Choy WY, Kay LE (1999) TROSY-based HNCO pulse sequences for the measurement of 1HN-15N, 15N–13CO, 1HN-13CO, 13CO-13Ca and 1HN-13Ca dipolar couplings in 15N, 13C, 2H-labeled proteins. J Biomol NMR 14:333–343

Zweckstetter M, Bax A (2000) Prediction of sterically induced alignment in a dilute liquid crystalline phase: aid to protein structure determination by NMR. J Am Chem Soc 122:3791–3792